Calibration and Estimation of Attitude Errors for a Rotating Fan-Beam Scatterometer Using Calibration Ground Stations

Jintai Zhu, Xiaolong Dong, *Senior Member, IEEE,* Wenming Lin, and Xingou Xu

***Abstract*—The rotating fan-beam scatterometer (RFSCAT) onboard Chinese-French Oceanic SATellite (CFOSAT) due to launch in 2018 is a new type of radar scatterometer system for ocean surface wind vector measurement. It can give observations with more azimuth and incidence angles for a single wind vector cell (WVC) than other available scatterometers. This has been proved effective in bettering the retrieved wind quality by the simulation approach. However, its innovative observing geometry is challenging for the coming in-orbit external calibration. In this paper, CFOSAT attitude errors are estimated, and its antenna gain pattern is monitored and verified based on the external calibration strategy of a Ku-band scatterometer employing calibration ground stations (CGSs). The effects of satellite attitude errors on the measurements are also analyzed, together with simulation results for the external calibration. It is shown that a gain pattern with accuracy of 0.08 dB and attitude errors within 0.025° are achieved.**

***Index Terms*—Attitude errors, calibration, calibration ground station (CGS), rotating fan-beam scatterometer (RFSCAT).**

I. Introduction

THE NORMALIZED radar cross section (NRCS, σ^0) measurements gained by spaceborne scatterometers have been successfully applied for wind field retrieving. Results estimated from a set of measured σ^0 highly rely upon the accuracy of σ^0 measurements. Thus, postlaunch calibration and verification have been drawn more attention for all the past and present scatterometers. The first scatterometer in space was SEASAT-A Scatterometer System (SASS) onboard SEASAT-A satellite in 1978. After the success of SASS, the advanced microwave instrument (AMI) on European Remote Sensing Satellite ERS-1 and ERS-2 were launched in 1991 and 1995, respectively. The National Aeronautics and Space Administration (NASA) SCATterometer (NSCAT), which was launched in 1996 flown on the ADEOS-1 satellite, was cut short by the loss of the host satellite in 1997. As a follow-up to this mission, NASA developed a new kind of scatterometer, SeaWinds, which used rotating pencil-beam instead of the multiple fixed fan-beams of SASS and NSCAT. SeaWinds had been successfully flown on QuikSCAT and ADEOS-2. After AMI, Advanced SCATterometer (ASCAT) onboard METOP-A and METOP-B satellites were launched by European Space Agency (ESA) in 2006 and 2012. Recently launched Oceansat-2 SCATterometer (OSCAT) by the Indian Space Research Organization (ISRO) and HY-2 SCATterometer (SCAT) by China's National Satellite Ocean Application Service (NSOAS) also succeeded in providing sea surface wind vector data. All the ESA-developed scatterometers, including AMI and ASCAT, operate at C-band, while others at Ku-band.

Up to now, operational scatterometers can be classified into two different types: 1) multiple fixed fan-beam scatterometers (SEASAT-A/SASS, ADEOS-1/NSCAT, ERS/AMI, METOP/ASCAT) and 2) rotating pencil-beam scatterometers (QuikSCAT/SeaWinds, ADEOS-2/SeaWinds, Oceansat-2/OSCAT, and HY-2/SCAT). Rotating fan-beam scatterometer (RFSCAT) is a new type that has more flexible views and larger observing swaths than fixed fan-beam ones, thus have more advantages in removing ambiguous solutions for wind retrieving [1], [2]. Moreover, it is not necessary to consider its beam balance for RFSCAT, which is an important issue for multiple fixed fan-beam scatterometers [3], [4]. Compared with rotating pencil-beam scatterometer, RFSCAT can also give more diverse observing views, since the spinning rate of RFSCAT antenna is much lower than rotating pencil-beam type, which also shows a potential improvement for the retrieval performance of wind direction [2], [5].

The preliminary requirement of RFSCAT calibration is consistent with QuikSCAT and its prior sensors, which demands an accuracy of 10% or ± 2 m/s for wind speed and $\pm 20°$ for wind direction retrieval [6]. In-orbit calibration is one of the most essential parts to achieve such accuracy. For RFSCAT, this is realized by calibrations of in-orbit antenna gain pattern, especially the elevation parts, and satellite attitude errors estimation as well [3].

Generally, three kinds of approaches can be adopted for scatterometers in-orbit calibration to get an accurate gain pattern: employing 1) active/passive calibration ground stations (CGSs) [7]–[9]; 2) homogeneous land targets [10]–[12]; and 3) ocean calibration method [4], [13]. Among them, active CGSs, i.e., transponders, provide very accurately known point target cross sections and have been used by AMI, ASCAT, and NSCAT [7],

Manuscript received December 11, 2013; revised March 30, 2014; accepted May 08, 2014. Date of publication May 28, 2014; date of current version February 04, 2015.

J. Zhu is with the Key Laboratory of Microwave Remote Sensing, National Space Science Center, Chinese Academy of Sciences, Beijing 100190, China, and also with the University of Chinese Academy of Sciences, Beijing 100049, China (e-mail: jintai.hust@gmail.com).

X. Dong and X. Xu are with the Key Laboratory of Microwave Remote Sensing, National Space Science Center, Chinese Academy of Sciences, Beijing 100190, China (e-mail: dongxiaolong@mirslab.cn).

W. Lin is with the Institute of Marine Sciences (ICM-CSIC), 08003 Barcelona, Spain.

Color versions of one or more of the figures in this paper are available online at http://ieeexplore.ieee.org.

Digital Object Identifier 10.1109/JSTARS.2014.2323993

[9]. Passive CGS, i.e., the CGS that does not transmit pulses to the radar instruments but just listens and records the instrument signals with satellites being unaware of its existence [8], [14], was firstly adopted by QuikSCAT and SeaWinds.

This paper aims at designing suitable calibration procedures for the coming RFSCAT onboard Chinese-French Oceanic SATellite (CFOSAT) due to launch in 2018. Effects of the satellite attitude errors on the calibration factor as well as σ^0 are analyzed based on the parameters of the RFSCAT onboard CFOSAT. A simple calibration model based on CGSs is proposed and verified by simulation to estimate each kind of errors contribution to the backscattering measurements. In Section II, measurement characteristics of this RFSCAT are described. The effects of satellite attitude errors over RFSCAT calibration are presented in Section III. Section IV introduces the calibration model using CGSs. Simulation results are then presented based on analysis employing three passive CGSs. Finally, conclusions are summarized.

II. Instrumentation

The scatterometer onboard CFOSAT will be the first spaceborne RFSCAT for global ocean surface wind vector measurement in application. The proposed scatterometer is a dual-beam radar (VV and HH polarized fan-beams) operating at Ku-band (13.256 GHz) and flying on a polar-orbit at an altitude of 519 km. The observation geometry of RFSCAT is shown in Fig. 1. It transmits long pulses with linear frequency modulation, maps power spectrum from the received echoes, and achieves fine range resolution of about several-hundred meters. Resolutions in azimuth dimension are determined by the antenna beamwidth. Signals are further averaged in the elevation direction into 5-km resolution cells before being transmitted to ground together with the data of noise measurements and internal calibration. The above-mentioned processing is adopted to reduce the data amount transmission in the link between satellite and ground segment. The dual-polarized (VV and HH) beams observe ocean surface at angles ranging $26^\circ \sim 51^\circ$ off-nadir with a mean platform altitude of 519 km together, ensures an observation swath of more than 1000 km.

There are a number of factors affecting the RFSCAT measurement accuracy: 1) in-orbit antenna gain pattern, especially the gain pattern in the elevation direction; 2) antenna gain fluctuation due to the rotary joint; and 3) satellite attitude errors [3]. In this paper, we mainly consider issues 1) and 3), while issue 2) can be removed using, e.g., tropical rain forest backscattering. Rain forests (e.g., Amazon rainforest) exhibit remarkably homogeneous in their radar responses over a very large area despite some spatial variability that can be ignored when a region of spatially homogeneous response is carefully selected [15]. Based on the calibrated antenna gain pattern and transmitted power monitored by the internal calibration loop, variations of the measured NRCS of the rain forest at certain points within the footprint will be evaluated at different azimuth looking angles, then the antenna gain fluctuation due to the rotary joint can be estimated [12], [16].

The antenna gain pattern of RFSCAT is to be calibrated using CGSs. To achieve high accuracy, the scatterometer would be operating in a special calibration mode that can be realized in two ways. First, as the antenna spinning rate remains the same as common mode (3.5 revolutions per minute), the pulse repetition frequency (PRF) of calibration mode is set to be not less than 300 Hz, in order to meet the requirement of sampling interval of 0.05°. The PRF is much higher than that in normal mode (150 Hz). An alternative progress is to make the antenna stop spinning and operate at a fixed azimuth position; this requires a PRF of no less than 15 Hz, which is decided by the ground speed of the satellite [3]. The latter is employed in the method proposed in this paper to avoid modification of the hardware system, since PRF in this calibration mode can be kept the same as that of normal mode, and CGS receives 75 pulses per second from each antenna beam. A few minutes prior to illumination by RFSCAT, the CGS's antenna would be steered to the predicted direction perpendicular to the satellite flight direction, and started to listen to the RFSCAT transmissions passively. Meanwhile the scatterometer would be switched into calibration mode, its antenna would stop spinning gradually and fixed at the side-looking direction finally. As soon as the CGS detects the characteristic signals transmitted by RFSCAT, it would begin recording the received pulse data.

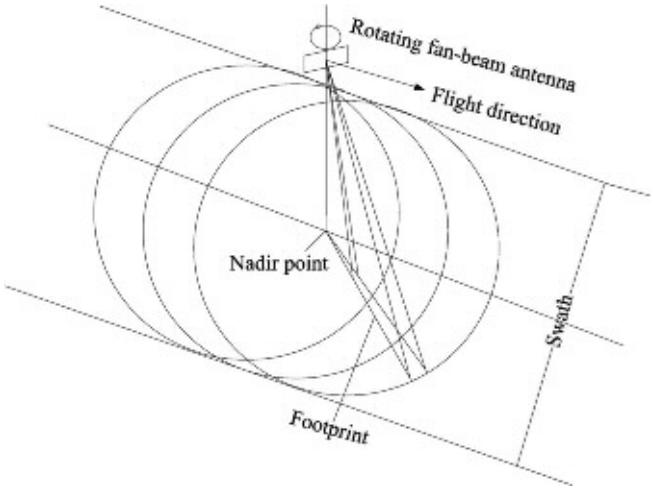

Fig. 1. Observe geometry of RFSCAT.

III. The Requirement of Calibration Attitude Errors

The scatterometer transmits an electromagnetic pulse to the surface and measures the echo power (P_R, the backscattered signal with additive noise). To compute the backscattered signal power P_S, a separate noise-only measurement channel is designed to acquire the noise power P_N. Thus, P_S is evaluated by $P_R - P_N$. The NRCS is calculated from the radar equation [10]

$$\sigma^0 = P_S / X \tag{1}$$

where X is the calibration factor [10]

$$X = \frac{\lambda^2 P_t}{(4\pi)^3 L_{\text{sys}}} \int \frac{G^2_{\text{scat}}(x) F(x)}{R^4(x)}\, dx \tag{2}$$

where P_t is the transmitted power, λ is the wavelength of the transmitted signal, and L_{sys} is the system losses, including

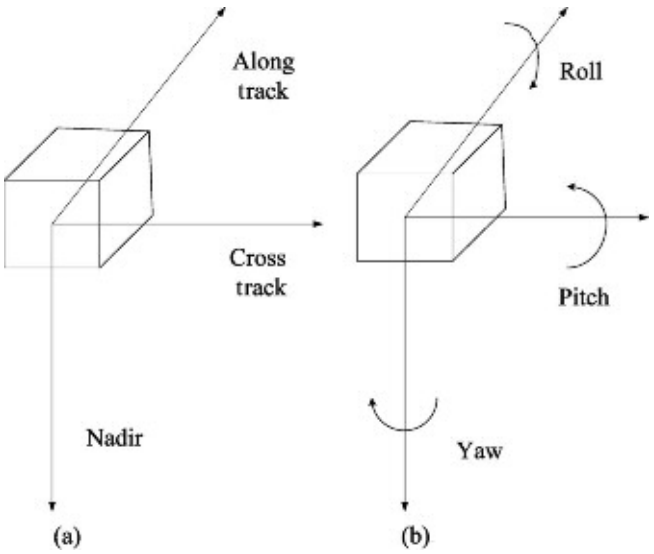

Fig. 2. Attitude definition sketches the (a) satellite position and (b) satellite attitude.

atmospheric loss and the transmission loss associated with the transmitting/receiving channels. x denotes the location of observation, $G_{\text{scat}}(x)$ is the scatterometer antenna gain, $R(x)$ is the slant range from the scatterometer to the observed scene, and $F(x)$ is the response function of the system filter.

As satellite attitude changes, the integral interval on the right side of (2) changes as well due to displacement of illumination of the antenna beam over ground areas. Unknown attitude errors will cause errors in X factor, and consequently errors in σ^0, which need to be well determined during the data processing. The attitude is usually expressed in terms of roll, pitch, and yaw, defined in Fig. 2 [17].

When the beam is in the along-track direction, the existence of pitch angle (θ_p) will lead the broad scatterometer antenna beam center deviate from the predetermined angle which occurs mainly in the elevation direction. The roll angle (θ_r) functions similarly when the beam is in the cross-track direction. Both of them will introduce estimating errors of the antenna gain and finally into X factor.

The satellite yaw angle (θ_y) is related with the beam azimuth angle (θ_{azi}) directly as

$$\theta_{\text{azi}} = \omega t + \theta_y \tag{3}$$

where ω is the antenna spinning rate in radians and t is observing time. θ_y introduces errors for both antenna azimuth position and Doppler frequency estimation. These, in turn, result in errors in X factor and the spatial orientation of the resolution cells.

The X factor errors act as a function of attitude errors and can be estimated in (2) using the actual RFSCAT antenna pattern that measured prelaunch in laboratory. While estimating the X factor errors due to attitude errors in one of the pitch, roll, and yaw angles, the errors in the respective other two parameters are kept zero. Fig. 3 illustrates the X factor errors when the pitch angle θ_p is presented while the broad beam of RFSCAT is pointing in different look directions. The relations between the X factor errors and the roll angle θ_r are expressed in Fig. 4. The contour lines display the X factor errors in decibel. Figs. 3 and 4 are

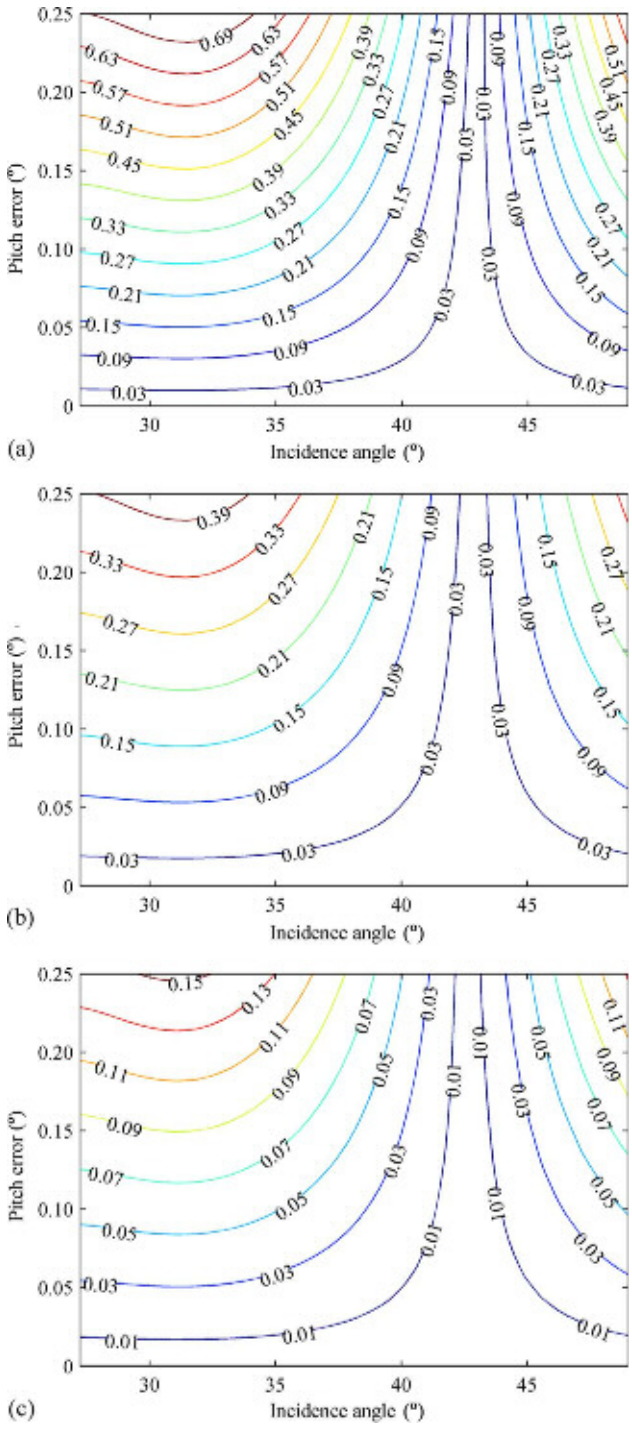

Fig. 3. Relationship between X factor errors (equivalently, σ^0 errors) and attitude errors caused by pitch angles when the beam is (a) in the along-track direction; (b) in the middle of side-swath direction; and (c) in the cross-track direction, respectively.

plotted with the subsatellite position near the equator. It can be observed that the X factor errors are lowest near the boresight direction, and getting larger when moving from the main lobe to side lobes in the elevation direction. Therefore, the resolution cells near the beam center have gain pattern of higher calibration accuracy, whereas lower values appear far away from the beam center. The X factor errors caused by pitch angles are maximum when the beam is in the along-track direction, and getting smaller

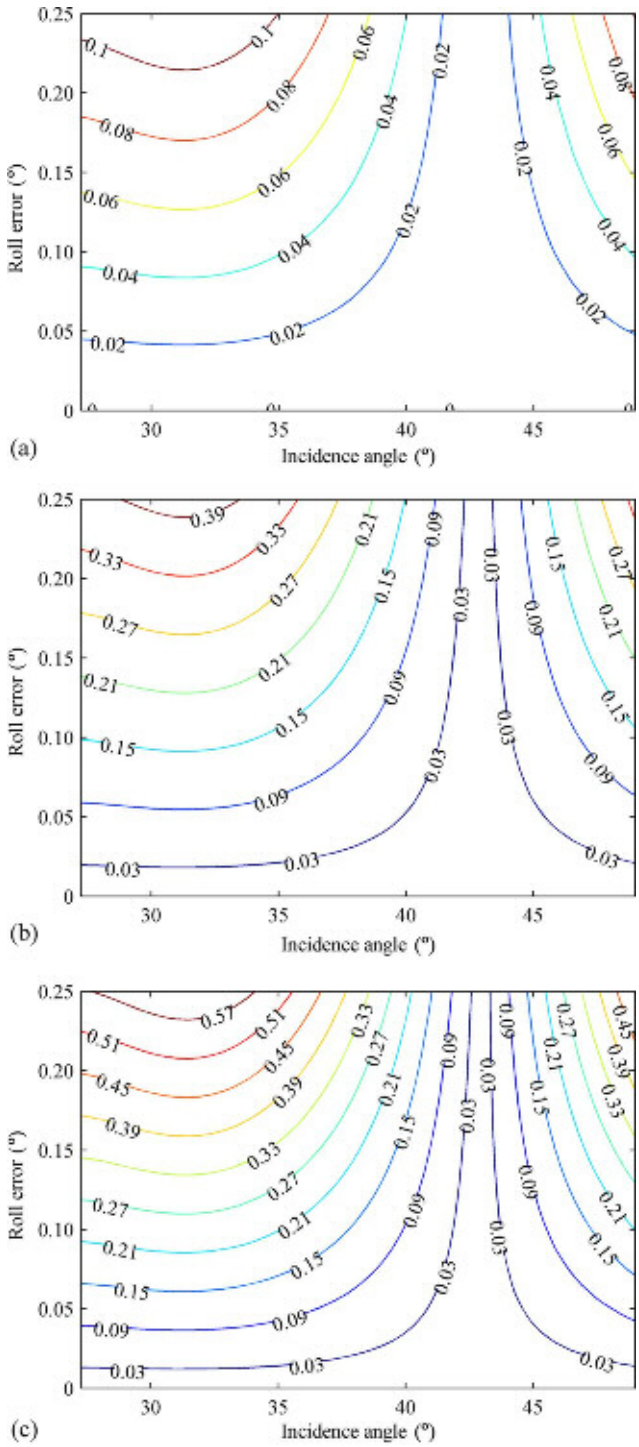

Fig. 4 Relationship between X factor errors and attitude errors caused by roll angles when the beam is (a) in the along-track direction; (b) in the middle of side-swath direction; and (c) in the cross-track direction, respectively.

as the antenna rotates until when the beam is in the cross-track direction, the values are minimum. Contrary to the X factor errors caused by pitch angles, those caused by roll angles are minimum when the beam is in the along-track direction and maximum when the beam is in the cross-track direction.

Fig. 5 shows the relationship between the yaw angle θ_y and the X factor errors, as well as the spatial orientation errors in the azimuth direction for ground resolution cells. The beam is assumed to be in the cross-track direction and the corresponding subsatellite position is at the equator. The X factor errors vary similarly as the antenna rotates with those caused by roll angles. The subresolution cells in a footprint realized by signal processing, i.e., slices, are numbered according to their positions within the footprint. Slice 1 is closest to the nadir, slice 32 is near the boresight of the antenna beam, and slice 57 locates farthest to the nadir. The spatial orientation errors increase as the slice number becomes larger. The relationship between attitude errors and the X factor errors vary with latitudes due to the changing slant ranges R with the latitudes [18].

It can be observed that the X factor is more sensitive to the attitude variations inducing a movement of antenna gain pattern in the elevation direction than that in the azimuth direction. To achieve the desired calibration accuracy of 0.15 dB for all the measurements within the footprint, satellite attitude knowledge of the order of 0.1° is necessary, which could be achieved through the following method.

IV. Calibration Method

A. Data Analysis Method

The parameters of the CGS proposed in this paper are listed in Table I, which are selected considering a wide main beam to minimize sensitivity to CGS pointing errors. The RFSCAT transmits different linear polarized signals (HH and VV). Differentiating signal polarizations will increase the complexity of the CGS system. A circular-polarized antenna has been adopted in this paper for it could always detect signals in different polarizations, though the signal power that the CGS received would be reduced.

Three CGSs are assumed to be applied located at T1 (95°E, 40°N), T2 (96°E, 40°N), and T3 (97°E, 40°N), respectively. Based on the CFOSAT orbit parameters and the locations of CGSs, the simulated pulse number that is acquired by CGSs during a 13-day ground-track repeat cycle would be more than 6000, i.e., 6000 simulated pulse samples per 197 orbits. Not all the data measured during a 13-day period are used for calibration. The side lobes of the RFSCAT antenna gain pattern that the CGS measured would be too small in values, whereas the effects of thermal noise on CGS received signals become relatively very strong. A threshold is set to filter out the data under the level. According to the configuration requirements of RFSCAT antenna [19], all the measurements with respect to the scatterometer antenna gain greater than 20 dB could be adopted by the algorithm below for estimation.

The CGS-received power is calculated according to the RFSCAT telemetry, the positions of CGSs, and the actual antenna patterns of both RFSCAT and CGSs. The governing equation is the one-way radar equation [7]

$$P_{\mathrm{Rcgs}} = \frac{\lambda^2 P_t G_{\mathrm{scat}} G_{\mathrm{cgs}}}{(4\pi)^2 R^2 L_{\mathrm{sys}}} + P_n \tag{4}$$

where P_{Rcgs} is the power measured by CGSs, P_t is the transmitted power, λ is the wavelength of the signal transmitted by the scatterometer, G_{scat} is the RFSCAT antenna gain, G_{cgs} represents the antenna gain of CGS, R is the slant range from the

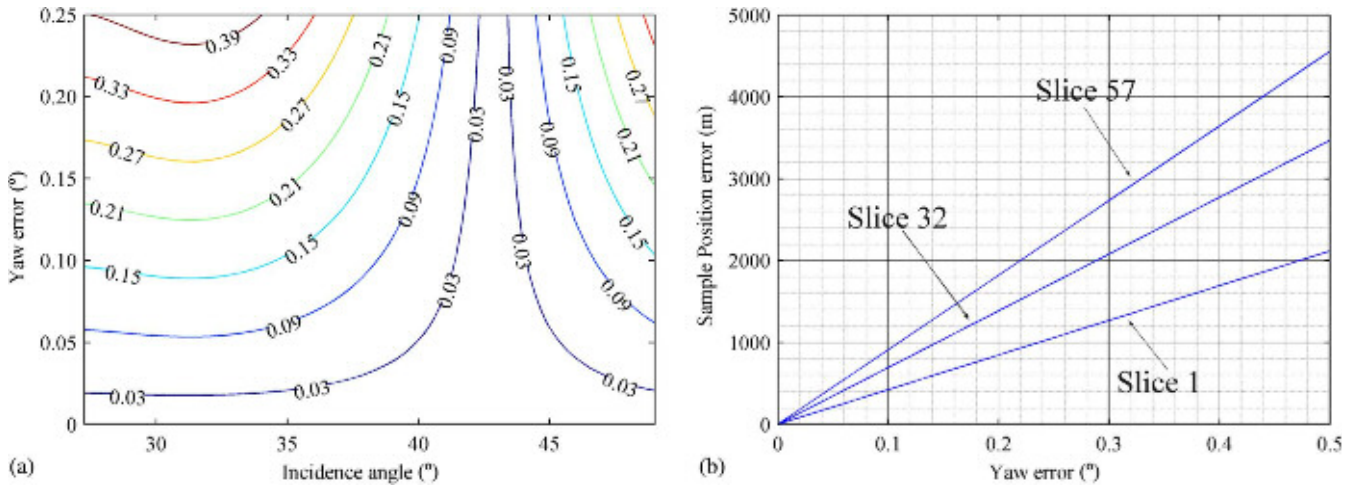

Fig. 5. Relationship between attitude errors (θ_y) and (a) the X factor errors and (b) the spatial orientation errors in the azimuth direction for the ground resolution cells when the beam is in the cross-track direction.

TABLE I
SYSTEM PARAMETERS OF THE CGS

Parameters	Values
Antenna beamwidth	13° within 3 dB
Antenna polarization	Circular polarization
Bandwidth of the received signal	500 kHz
System noise temperature	290 K

scatterometer to the CGS, and $L_{\rm sys}$ is the system losses of CGSs, including atmospheric loss and the transmission loss associated with the CGS's receiving channel. $P_n = kTB$ is the thermal noise in the receiving system of CGS. k is the Boltzmann constant. T and B are the system noise temperature and system bandwidth of the CGS's receiver, respectively. According to (4), the signal-to-noise ratio (SNR) in the CGS's receiver can be approximated as follows:

$$\mathrm{SNR} = \frac{\lambda^2 P_t G_{\rm scat} G_{\rm cgs}}{(4\pi)^2 R^2 L_{\rm sys} P_n}. \tag{5}$$

To analyze the attitude errors impacts over the scatterometer antenna gain pattern, we assumed that all the terms on the right side of (4), except $G_{\rm scat}$, $G_{\rm cgs}$, and R, were constant in the duration of a beam sweep. The value of $G_{\rm cgs}$ was interpolated from the premeasured gain pattern in the CGSs' looking direction, which could be determined by their positions (from GPS), commanded pointing directions and satellite position (from the predicted ephemeris). The CGSs' measurements used in the algorithm corresponding to antenna gain of scatterometer are greater than 20 dB, which typically have a SNR value of 30 dB or higher calculated using (5). Thus, the noise power P_n was negligible in this algorithm. The mean SNR values of CGSs' measurements averaged over azimuth angles at different incidence angles is shown in Fig. 6.

The scatterometer gain pattern was estimated by transferring (4) into the following form

$$G_{\rm scat}(\theta,\varphi) = \frac{P_{\rm Rcgs}}{P_t}\frac{(4\pi)^2 R^2 L_{\rm sys}}{\lambda^2 G_{\rm cgs}}. \tag{6}$$

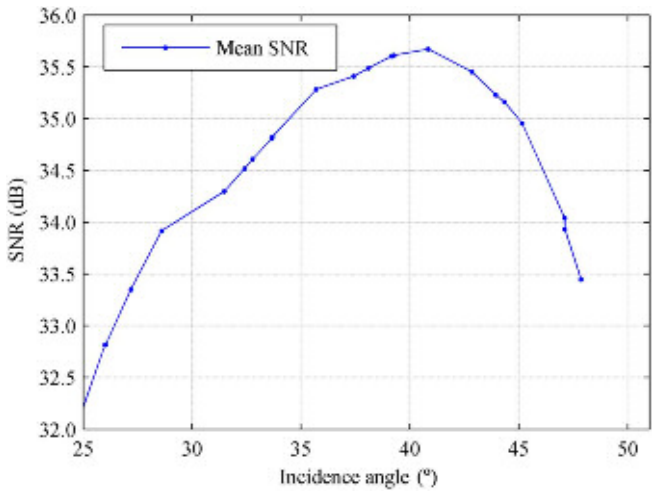

Fig. 6. Mean SNR values of the CGS samples at different incidence angles that used in the calibration algorithm.

The accuracy of estimated antenna gain pattern was determined by the knowledge of observing geometry calculated according to satellite position (from the ephemeris), satellite attitude, RFSCAT antenna deployment accuracy, and the CGSs' positions (provided by GPS) [7]. $P_{\rm Rcgs}$ is perturbed by thermal noise of its receiving system, thus the occasional spurious signals are filtered out prior to the calculation of scatterometer antenna gain using (6).

The actual antenna gain of RFSCAT in the nominal antenna coordinates $G_{\rm ACT}(\theta_N,\varphi_N)$ was modeled as follows [20]:

$$G_{\rm ACT}(\theta_N,\varphi_N) = G_{\rm DIS}(\theta_N,\varphi_N,c_{\rm nm},\theta_r,\theta_y,\theta_p) + G_{\rm NOM}(\theta_N,\varphi_N,\theta_r,\theta_y,\theta_p)(\mathrm{dB}) \tag{7}$$

where $G_{\rm DIS}$ is the estimated antenna gain distortion function, which is mainly due to mechanical and thermal deformation of the antenna and the observing geometry fluctuations caused by satellite attitude errors. $G_{\rm NOM}$ is the prelaunch determined antenna pattern. The postlaunch gain pattern was modeled as a function of actual RFSCAT antenna coordinate in-orbit

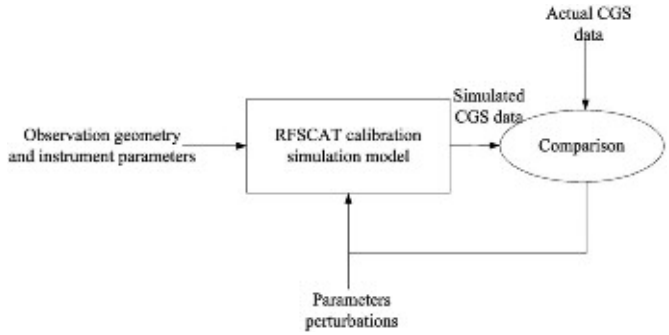

Fig. 7. Flow diagram of the RFSCAT simulation process.

(θ_N, φ_N), and the satellite roll, yaw, and pitch angle: θ_r, θ_y, θ_p. $\mathrm{c_{nm}}$ is one of the parameters of G_{DIS} given below, which is initially unknown but could be estimated from the CGS measured data $G_{\mathrm{MEAS}}(\theta_N, \varphi_N)$.

The variation of the RFSCAT antenna gain pattern at point $(\theta_N, \varphi_N, \theta_r, \theta_y, \theta_p)$, G_{DIS}, is compared to the prelaunch antenna pattern. The main lobe of the RFSCAT antenna gain pattern is mainly interested in the in-orbit calibration and it is a smooth surface. For the small in-orbit variation expected for RFSCAT at point $(\theta_N, \varphi_N, \theta_r, \theta_y, \theta_p)$, it could be expressed by a polynomial model

$$G_{\mathrm{DIS}}(\theta_{\mathrm{ACT}}, \varphi_{\mathrm{ACT}}, c_{\mathrm{nm}}) = \sum_m \sum_n c_{\mathrm{nm}} \theta_{\mathrm{ACT}}^m \varphi_{\mathrm{ACT}}^n \qquad (8)$$

where $\mathrm{c_{nm}}$ are the coefficients of the antenna gain distortion function. m and n denote the orders of polynomial model in the elevation direction and in the azimuth direction of RFSCAT antenna, respectively. $(\theta_{\mathrm{ACT}}, \varphi_{\mathrm{ACT}})$ are functions of nominal antenna frame coordinates (θ_N, φ_N) and satellite attitude errors as follows:

$$\begin{aligned} \theta_{\mathrm{ACT}} &= f_1\big(\theta_N, \varphi_N, \theta_r, \theta_y, \theta_p\big) \\ \varphi_{\mathrm{ACT}} &= f_2\big(\theta_N, \varphi_N, \theta_r, \theta_y, \theta_p\big). \end{aligned} \qquad (9)$$

The attitude errors affect the point at $(\theta_N, \varphi_N, \theta_r, \theta_y, \theta_p)$ in the actual antenna frame coordinates, and in turn affect the antenna gain distortion function. After attitude errors had been assessed, simulation model could be perturbed by the estimated results. Then resimulation could be conducted. The next step is to re-estimate coefficients of the antenna gain distortion function c_{nm}. Fig. 7 shows the simulation process for calibrating the RFSCAT antenna gain pattern. The simulation processes are described as follows.

1) Satellite passes each CGS.
2) CGS detects the RFSCAT signals, listens, and records the pulse data.
3) Data processing, comparing the simulated data with the actual CGS measured data.
4) Attitude errors estimation.
5) Final RFSCAT antenna gain pattern estimation.
6) The reporting of the calibration analysis results.

B. Attitude Errors Estimation

Attitude errors estimations would be difficult due to the many-to-one mapping from the RFSCAT antenna gain pattern to the received power, meaning there are many values of $(\theta_N, \varphi_N, \theta_r, \theta_y, \theta_p)$ which correspond to the same antenna gain value [14]. Fig. 8 shows the simulated RFSCAT antenna gain pattern for a selected CGS sweep and the effects of attitude errors on the antenna gain (error of 0.5°). Estimations of attitude errors are also limited by the knowledge of satellite and CGS positions as well as other possible differences between the model and actual operation.

With actual antenna gain pattern unknown which would be dependent on satellite attitude, the desire for an unbiased estimator is conducted in a variance-based approach. There are four free parameters in the model, θ_r, θ_y, θ_p, and antenna gain distortion factor S, which is a constant related to the antenna gain distortion function and used with (7) to estimate the attitude errors due to unknown antenna gain distortion function. The objective function F_1 is

$$\begin{aligned} F_1\big(\theta_r, \theta_y, \theta_p, S\big) = \frac{1}{N_m} \sum_{i=1}^{N_m} &\big[G_{\mathrm{MEAS}}(\theta_N(i), \varphi_N(i)) \\ &- G_{\mathrm{MODEL}}(\theta_N(i), \varphi_N(i))\big]^2 \end{aligned} \qquad (10)$$

where N_m is the CGS-measured pulses number that is used in the estimation algorithm, G_{MEAS} is the actual CGS measured data, and G_{MODEL} is the simulated CGS data given in (7), where the antenna gain distortion function is replaced by antenna gain distortion factor S. The estimation of $\mathbf{a} = [\theta_r, \theta_y, \theta_{p,} S]$ is thus given by

$$\widehat{\mathbf{a}} = \arg\min_{\mathbf{a}} \{F_1(\mathbf{a})\}. \qquad (11)$$

The objective function of (11) is minimum when the estimated attitude errors are close to the actual situation. Minimization of the objective function was performed by employing trust-region-reflective algorithm. The CFOSAT satellite platform has an attitude accuracy much better than within $\pm 1^\circ$ [21]. During the estimation, we assume the attitude errors within $\pm 1^\circ$.

C. Antenna Gain Pattern Estimation

When the attitude errors had been estimated, simulation model parameters would be perturbed by these estimations and resimulation could be conducted. Antenna gain pattern is then calibrated using trust-region-reflective algorithm. The outputs of this algorithm are the coefficients of the antenna gain distortion function. The objective function F_2 is

$$F_2(c_{\mathrm{nm}}) = \frac{1}{N_m} \sum^{N_m} \left(G_{\mathrm{DIF}} - G_{\mathrm{DIS}}\right)^2 \qquad (12)$$

where $\mathrm{G_{DIF}}$ is the difference between CGS measured data and the normal antenna gain pattern. $\mathrm{G_{DIF}}$ is given by

$$\begin{aligned} G_{\mathrm{DIF}}(\theta_N, \varphi_N) = &G_{\mathrm{MEAS}}(\theta_N, \varphi_N) \\ &- G_{\mathrm{NOM}}\Big(\theta_N, \varphi_N, \theta_r^{est}, \theta_y^{est}, \theta_p^{est}\Big) \end{aligned} \qquad (13)$$

where θ_r^{est}, θ_y^{est}, and θ_p^{est} are the estimated attitude errors of θ_r, θ_y, and θ_p, respectively, using (11). The estimation of c_{nm} is thus

$$c_{\mathrm{nm}} = \arg\min\{F_2(c_{\mathrm{nm}})\}. \qquad (14)$$

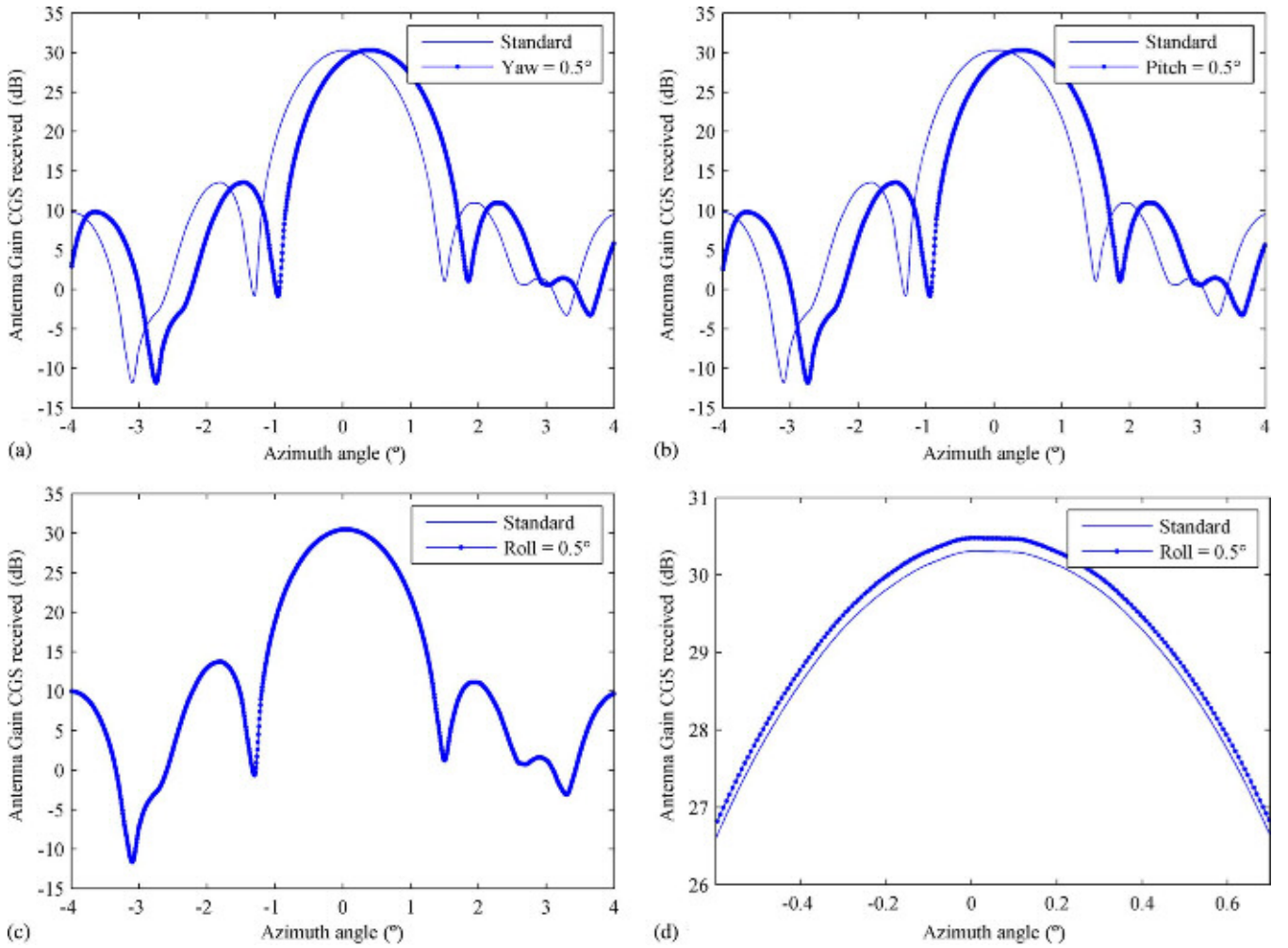

Fig. 8. Simulated CGS sweep showing the effects of attitude errors. (a) Yaw angle. (b) Pitch angle. (c) Roll angle. (d) Zooms in the plot of (c).

Minimizing the objective function in (14), the coefficients of the antenna gain distortion function are estimated. Finally, the antenna gain pattern could be derived from the series of coefficients in (7). The root mean square (rms) residual of antenna gain pattern is used to evaluate this estimation. The rms of the antenna gain pattern is calculated using

$$\text{RMS} = \sqrt{\frac{1}{N_m}\sum_{i=1}^{N_m}\left(G_{\text{MEAS}}(\theta_N(i),\varphi_N(i)) - G_{\text{MODEL}}(\theta_N(i),\varphi_N(i))\right)^2}. \tag{15}$$

First, the coefficient of the antenna gain distortion function c_{00} is estimated. Then the orders of the polynomial is gradually increased, and the estimation is conducted in further iteration until the rms of the antenna gain pattern would be small enough or not get smaller obviously. At particular values of m and n, the rms of the antenna gain pattern is the minimum and these values of m and n were opted for the final choices for m and n. Finally, the orders of the polynomial m and n are determined and the coefficients of the antenna gain distortion function c_{nm} could be estimated.

Bias errors would always exist in the determined ephemeris and then it would be introduced into antenna gain estimation error, which can be calculated using (16)

$$10\log_{10}\left(1+\frac{\Delta G_{\text{slant}}}{G}\right) = 10\log_{10}\left(1+\frac{2\Delta R}{R}\right) \tag{16}$$

where ΔR is the bias error of slant range due to a bias error in the determined ephemeris and ΔG_{slant} is the bias error of antenna gain pattern G that is introduced by ΔR. This would be discussed in Section V.

Atmospheric loss would be another error that should be considered. The total errors of the calibration using this calibration algorithm can be calculated as follows:

$$\Delta\sigma^0_{\text{scat}} = \sqrt{\left(\Delta\sigma^0_{\text{point}}\right)^2 + \left(\Delta\sigma^0_{\text{DIS}}\right)^2 + \left(\Delta\sigma^0_{\text{slant}}\right)^2 + \left(\Delta\sigma^0_{\text{atm}}\right)^2} \tag{17}$$

where $\Delta\sigma^0_{\text{scat}}$ is the total errors of the antenna gain pattern estimated using this algorithm, $\Delta\sigma^0_{\text{point}}$ is the effects of attitude errors on X factors, $\Delta\sigma^0_{\text{DIS}}$ is introduced by residual of the estimation of antenna gain pattern, $\Delta\sigma^0_{\text{slant}}$ is the bias errors

introduced by slant range errors, and $\Delta\sigma^0_{\text{atm}}$ is the atmospheric loss.

V. Results and Analysis

All the data measured by CGSs are assumed to have been gained in the same angular position to be same in ascending and descending passes. Possible multipath effects are not included in this simulation, since they are one of the most important considerations in placement of CGSs and would be minimized during their installations. The slant range to the near swath edge for the RFSCAT on CFOSAT is always greater than 570 km. It is reasonable to assume that the determined ephemeris is supposed to have accuracy as 100 m. Then the bias error of slant range introduced into antenna gain error would be less than 0.0015 dB calculated according to (16). Atmospheric loss would be mainly related with oxygen content and water vapor density in the clear sky, which is another error source for the calibration. It could be reasonable to assume that one-way loss in the atmosphere per kilometer is about 0.0065 dB/km under the condition that the relative humidity is 30% lower [22]. The height of the atmosphere was assumed to be 12 km and the incidence angles of RFSCAT beams range from 26° to 51°. Thus, the atmospheric loss would vary between 0.0868 and 0.1239 dB. The constant part in atmospheric loss will be compensated in the data processing. Thus, the variation of atmospheric loss that would be introduced into antenna gain estimation error is about 0.0371 dB.

The RFSCAT footprint would sweep over the three CGSs 26 times during a 13-day period. Each time a set of data corresponding to a single incidence angle could be acquired. Every single incidence observation consisted of approximately 200 samples in the along-track direction, which was estimated by simulation. Finally, we would have acquired more than 5000 available samples of antenna gain pattern measurements covering the main lobe ($G_{\text{scat}} \geq 20$ dB) of the RFSCAT antenna pattern, as these samples have higher SNR.

The attitude errors would affect the antenna gain distortion function and they were estimated before the estimation of antenna gain pattern. The transmission equation (one-way) had been used to simulate the satellite and CGS contact situation. According to the simulation process in Fig. 7, the satellite attitude errors were estimated using the first model with corresponding objective function F_1. The simulation results indicated that the satellite attitude errors could be estimated with an accuracy of about $\pm 0.02°$ for θ_r, $\pm 0.01°$ for θ_y, and $\pm 0.001°$ for θ_p. The rms residual is less than 0.025°. Effects of attitude errors on the X factor as well as σ^0 were less than 0.05 dB (as Fig. 9). The spatial orientation error of the resolution cell is less than 200 m.

After attitude errors had been assessed, simulation model could be perturbed by the estimated results. Then resimulation could be conducted. The next step was to estimate the antenna gain pattern. Minimizing the objective function F_2, the coefficients of the antenna gain distortion function were estimated. First, the c_{00} coefficient was estimated and the rms of gain antenna pattern was calculated using (15). Then the higher order polynomial coefficients were estimated over further cycles according to the rms values until the rms of the antenna gain pattern would be small enough or not get smaller obviously. m was set as 7 and n as 9 for (9), since the rms of the antenna gain pattern was

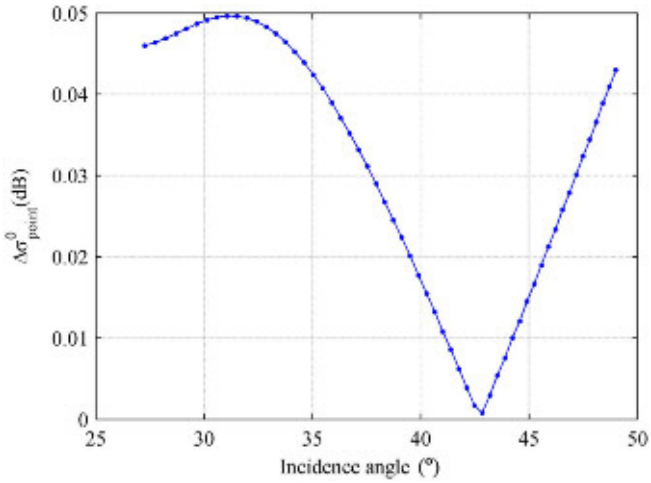

Fig. 9. Attitude estimation impact on X factor.

minimum at these particular values of m and n. Finally, the antenna gain pattern could be derived from the series of coefficients. Providing both attitude errors and the model coefficients, the antenna gain pattern can finally be estimated using (7). The rms residual of the estimation of antenna gain pattern was calculated using (15) resulted as less than 0.05 dB. Taking the slant range bias and atmospheric loss into account, the total errors of the antenna gain pattern was less than 0.08 dB.

VI. Summary and Conclusion

In this paper, basic considerations of calibrating a RFSCAT had been presented. Based on the CFOSAT parameters, the effects of the satellite attitude errors on the calibration factor and on σ^0 were analyzed. A simple calibration model based on CGSs was proposed and verified by simulation to estimate the contributions of each kind of errors to the backscattering measurements. The rms residual of estimated satellite attitude errors after calibration had achieved less than 0.025°. The effect of satellite errors on the calibration factor was less than 0.05 dB and the spatial orientation error was less than 200 m. The simulation results showed that the estimation accuracy of RFSCAT antenna gain pattern would be less than 0.08 dB, indicating that CGS-based calibration method was able to monitor and to verify the status of the RFSCAT antenna gain pattern effectively. This calibration approach could be used as a reference for the calibration of RFSCAT and other scatterometers.

There were 26 observations of three CGSs and the largest distance between adjacent two times was about 50 km. In the future, more CGS stations would be considered in order to reduce the distance between two passing duration to get better results. The weights of data used in the calibration could also be considered since measuring results may vary with different CGSs. And the next step of calibration for the RFSCAT on CFOSAT would be eliminating of joint insertion loss through rain forests.

References

[1] C. C. Lin *et al.*, "Wind retrieval capability of rotating range-gated fanbeam spaceborne scatterometer," in *Proc. SPIE*, Crete, Greece, 2003, vol. 4881, pp. 268–279.

[2] W. Lin and X. Dong, "Design and optimization of a Ku-band rotating, range-gated fanbeam scatterometer," *Int. J. Remote Sens.*, vol. 32, no. 8, pp. 2151–2171, Apr. 2011.
[3] X. Dong, D. Liu, J. Zhu, D. Zhu, and W. Lin "Some considerations about the in-orbit calibration of spaceborne rotating fan beam scatterometer," in *Proc. Int. Geosci. Remote Sens. Symp.*, Vancouver, Canada, 2011, pp. 965–968.
[4] A. Stoffelen, "A simple method for calibration of a scatterometer over the ocean," *J. Atmos. Ocean. Technol.*, vol. 16, pp. 275–282, Feb. 1999.
[5] X. Dong, D. Zhu, W. Lin, H. Liu, and J. Jiang, "A Ku-band rotating fan-beam scatterometer: Design and performance simulations," in *Proc. Int. Geosci. Remote Sens. Symp.*, Honolulu, HI, USA, 2010, pp. 1081–1084.
[6] C. L. Wu, Y. Liu, K. H. Kellogg, K. S. Pak, and R. L. Glenister, "Design and calibration of the SeaWinds scatterometer," *IEEE Trans. Aerosp. Electron. Syst.*, vol. 39, no. 1, pp. 94–109, Jan. 2003.
[7] R. D. West, W. Y. Tsai, J. L. Granger, and W. H. Daffer, "Calibration of the NASA Scatterometer using a ground calibration station," in *Proc. SPIE Earth Observ. Syst. III*. San Diego, CA, USA, 1998, vol. 3439, pp. 450–459.
[8] P. K. Yoho *et al.*, "SeaWinds on QuikSCAT calibration using a calibration ground station," in *Proc. Int. Geosci. Remote Sens. Symp.*, Honolulu, HI, USA, 2000, pp. 1039–1041.
[9] J. J. W. Wilson *et al.*, "Radiometric calibration of the advanced wind scatterometer radar ASCAT carried onboard the METOP-A satellite," *IEEE Trans. Geosci. Remote Sens.*, vol. 48, no. 8, pp. 3236–3255, Aug. 2010.
[10] D. G. Long and G. B. Skouson, "Calibration of spaceborne scatterometers using tropical rain forests," *IEEE Trans. Geosci. Remote Sens.*, vol. 34, no. 2, pp. 413–424, Mar. 1996.
[11] A. Elyouncha and X. Neyt, "C-band satellite scatterometers intercalibration," *IEEE Trans. Geosci. Remote Sens.*, vol. 51, no. 3, pp. 1478–1491, Mar. 2012.
[12] J. Zhu, X. Dong, W. Lin, and D. Zhu, "Calibration of the Ku-band rotating fan-beam scatterometer using land extended-area targets," *J. Electron. Inf. Technol.*, vol. 35, no. 8, pp. 1793–1799, Aug. 2013.
[13] C. Anderson *et al.*, "Validation of backscatter measurements from the advanced scatterometer on Metop-A," *J. Atmos. Ocean. Technol.*, vol. 29, no. 1, pp. 77–88, Jan. 2011.
[14] P. K. Yoho, "Satellite scatterometers: Calibration using a ground station and statiscal measurement theory," Ph.D. dissertation, Dept. Elect. Comput. Eng., Brigham Young Univ., Provo, UT, USA, 2003.
[15] R. G. Kennett and F. Li, "Seasat over-land scatterometer data. II. Selection of extended area and land-target sites for the calibration of spaceborne scatterometers," *IEEE Trans. Geosci. Remote Sens.*, vol. 27, no. 6, pp. 779–788, Nov. 1989.
[16] X. Dong, D. Zhu, J. Zhu, and T. Wang, "Progresses of development of CFOSAT scatterometer," in *Proc. Int. Geosci. Remote Sens. Symp.*, Munich, Germany, 2012, pp. 237–240.
[17] A. Anderson, "Analysis and usage of the QuikSCAT calibration ground station," M.S. thesis, Dept. Elect. Comput. Eng., Brigham Young Univ., Provo, UT, USA, 2001.
[18] M. W. Spencer, C. Wu, and D. G. Long, "Improved resolution backscatter measurements with the SeaWinds pencil-beam scatterometer," *IEEE Trans. Geosci. Remote Sens.*, vol. 38, no. 1, pp. 89–104, Jan. 2000.
[19] D. Zhu, X. Dong, W. Lin, and R. Yun, "Doppler effect and compensation in a Rotating Fanbeam Spaceborne Scatterometer," in *Proc. Int. Geosci. Remote Sens. Symp.*, Honolulu, HI, USA, 2010, pp. 1089–1091.
[20] J. J. W. Wilson, P. L. Phillips, J. F. Saldana, K. Dumper, and T. Fiksel, "Radiometric calibration of the advanced wind scatterometers carried onboard the METOP satellites," in *Proc. Int. Geosci. Remote Sens. Symp.*, Seoul, Korea, 2005, pp. 3436–3440.
[21] W. Lin, "Study on spaceborne rotating, range-gated, fanbeam scatterometer system," Ph.D. dissertation, Center for Space Science and Applied Research, Grad. Univ. Chinese Acad. Sci., Beijing, China, 2011.
[22] J. He, "Research of sounding, calibration and retrieval theory and techniques on microwave/millimeter-wave atmospheric temperature and humidity," Ph.D. dissertation, Center for Space Science and Applied Research, Grad. Univ. Chinese Acad. Sci., Beijing, China, 2012.

Jintai Zhu was born in Henan Province, China, on March 28, 1987. He received the B.S. degree in engineering from Huazhong University of Science and Technology, Wuhan, China, in 2009 and currently pursuing the Ph.D. degree in engineering from the University of Chinese Academy of Sciences, Beijing, China.

He is a Research Intern with the National Space Science Center, Chinese Academy of Sciences, Beijing, China, from 2010 working on the calibration of scatterometer.

Xiaolong Dong (A'01–SM'01) was born in Shaanxi Province, China, in 1969. He received the B.E. degree in radio technology and the Ph.D. degree in electromagnetic theory and microwave techniques, in 1991 and 1996, respectively, both from Xi'an Jiaotong University, Xi'an, China.

From 1996 to 1999, he was a Postdoctoral Research Fellow and an Associate Professor with the National Space Science Center, Chinese Academy of Sciences, Beijing, China, and promoted as a Full-Professor in 1999. From 2001 to 2003, he visited Duke University, Durham, NC, USA. Since November 2004, he has been a Hundred Talents Professor of the Chinese Academy of Sciences in the National Space Science Center, where he is now the Assistant Director-General of the Center and Deputy Director of the CAS Key Laboratory of Microwave Remote Sensing. He has been the Principal Investigator of the scatterometers of several Chinese oceanic observation satellites, including the Chiese-French Oceanic Satellite (CFOSAT) and the Haiyang-2 (HY-2) satellite. He is the author of more than 80 journal papers and conference presentation. His research interests include theory and techniques of microwave remote sensing, development of advanced microwave sensors, with emphasis on radar scatterometry for atmospheric, oceanic, and land surface applications.

Dr. Dong has been the Chair of the Microwave Sensors Subgroup of the Working Group on Calibration and Validation of the Committee of Earth Observation Satellites since 2008.

Wenming Lin was born in China, on April 22, 1984. He received the B.Sc. degree in engineering from Wuhan University, Wuhan, China, in 2006, and the Ph.D. degree in engineering from the Center for Space Science and Applied Research, Chinese Academy of Sciences, Beijing, China, in 2011.

He is currently a Postdoctoral Researcher with the Institute of Marine Sciences (ICM-CSIC), Barcelona, Spain, working on the scatterometer wind quality control.

Xingou Xu was born in China, on April 28, 1984. She received the B.S. degree in engineering from Wuhan University, Wuhan, China, the Dual B.A. degree in English from Huazhong University of Science and Technology, Wuhan, China, in 2005, and the Ph.D. degree in engineering from Wuhan University, in 2011.

From 2008 to 2009, she was a Visiting Researcher with the University of Edinburg, Edinburg, U.K. From 2011 to 2013, she was a Postdoctoral Researcher with the National Space Science Center, Chinese Academy of Sciences, Beijing, China. She is currently an Assistant Professor with the National Space Science Center working on the scatterometer data processing and simulation.